



# Bianchi type-III Tsallis holographic dark energy model in Saez–Ballester theory of gravitation

M. Vijaya Santhi<sup>a</sup>, Y. Sobhanbabu<sup>b</sup>

Department of Applied Mathematics, Andhra University, Visakhapatnam 530003, India

Received: 4 August 2020 / Accepted: 6 December 2020 / Published online: 24 December 2020  
© The Author(s) 2020

**Abstract** In this paper, we have investigated Tsallis holographic dark energy (infrared cutoff is the Hubble radius) in homogeneous and anisotropic Bianchi type-III Universe within the framework of Saez–Ballester scalar–tensor theory of gravitation. We have constructed non-interaction and interaction dark energy models by solving the Saez–Ballester field equations. To solve the field equations, we assume a relationship between the metric potentials of the model. We developed the various cosmological parameters (namely deceleration parameter  $q$ , equation of state parameter  $\omega_t$ , squared sound speed  $v_s^2$ , om-diagnostic parameter  $Om(z)$  and scalar field  $\phi$ ) and well-known cosmological planes (namely  $\omega_t - \omega_t'$  plane, where  $'$  denotes derivative with respect to  $\ln(a)$  and statefinders  $(r-s)$  plane) and analyzed their behavior through graphical representation for our both the models. It is also, quite interesting to mention here that the obtained results are coincide with the modern observational data.

## 1 Introduction

The current scenario of the accelerated expansion of the Universe confirmed through various observational schemes by Riess et al. [1,2]. Cosmological observations and Cosmic Microwave Background (CMB) data suggest [3,4] that the Universe is spatially flat and is dominated by an exotic component with huge negative pressure dubbed as Dark Energy (DE). It is also believed that DE occupies 73% of the energy of our Universe, Dark Matter (DM) occupies 23% and the 6% energy is baryonic matter [5,6]. In order to convey this late time acceleration, two main various approaches have been advocated: one is to construct different DE candidates and the second one is the modifications of Einstein's theory of gravitation. Among the many modifications, Brans–Dicke

[7] and Saez–Ballester [8] scalar–tensor theories played a significant role.

Saez and Ballester [8] introduced a scalar–tensor theory in which metric is combined with a dimensionless scalar-field was developed. This coupling is used to describe the weak fields satisfactorily. This scalar–tensor theory plays an important part in solving the issue of missing matter problem and in removing the graceful issue of exit in non-flat FRW cosmologies and the inflation era. In SB theory, the field equations are given by

$$R_{ij} - \frac{1}{2}Rg_{ij} - w\phi^n \left( \phi_{,i}\phi_{,j} - \frac{1}{2}g_{ij}\phi_{,k}\phi^{,k} \right) = -\frac{8\pi G}{c^4}T_{ij}, \quad (1)$$

and the scalar field ( $\phi$ ) satisfies the following equation

$$2\phi^n \phi_{,i}^i + n\phi^{n-1} \phi_{,k}\phi^{,k} = 0, \quad (2)$$

here  $T_{ij}$  is the energy momentum tensor of the matter, the gravitational constant  $G$ ,  $w$  is a dimensionless constant and, comma (,) and semicolon (;) represents partial and covariant differentiation respectively. The energy-conservation equation is given by

$$T_{;j}^{ij} = 0. \quad (3)$$

In past years, the holographic principle had attracted considerable attention due to its importance in quantum gravity [9–11], which is defined as the entropy of a given system which does not depend upon the volume, but rather on the surface area surrounding it. In the cosmological context, the holographic principle establishes an upper limit for the entropy of the Universe and there is a theoretical relation between IR and Ultraviolet (UV) cutoffs. If there is an energy density ( $\rho_{de}$ ) in a region associated to the UV, then the total energy in a phase of size  $L$  cannot be greater than the mass of a black hole with the same size, so that [12],  $L^3 \rho_{de} > LM_p^2$ .

<sup>a</sup> e-mail: [gv.santhi@live.com](mailto:gv.santhi@live.com) (corresponding author)

<sup>b</sup> e-mail: [sobhan.maths@gmail.com](mailto:sobhan.maths@gmail.com)

In this case, the largest value of  $L$  can be obtained by considering the equality in equation such that the holographic energy density is given by  $\rho_{de} = 3c^2 M_p^2 L^{-2}$ , where  $c$  is a numerical constant and  $M_p^2 = 8\pi G$  is the reduced Planck mass. Li [13] has shown that Hubble horizons and particle horizons are not in good agreement with the Universe while the future event horizon is the best model for non-interacting holographic DE with suitable constant  $c$ . Gao et al. [14] have pointed out that holographic DE with future event horizon is plagued with causality problem. Inspired by this, several authors have modified the IR cutoff as a function of the Ricci scalar [15, 16]. Since the energy density of the holographic DE is based on the area law of entropy, any modification of the area law leads to a modified holographic DE. The entropy expression is associated with the apparent horizon of FRW Universe in DGP braneworld motivated Sheykhi et al. [17] to introduce a new model for the holographic DE known as New Holographic DE (NHDE). They have investigated the cosmological consequences of this NHDE model by choosing the Hubble radius  $L = H^{-1}$  as the system's IR cutoff and have proved that it can explain the current cosmic acceleration of the Universe.

Nojiri and Odintsov [18] have proposed a unifying approach to early-time and late-time Universe based on phantom cosmology is proposed. Also, they have discussed the bound for holographic entropy which decreases in phantom era. Medved [19] has given a comment on holographic DE and mentioned that their interpretation of the DE turns out to be suggestive of a natural resolution to the cosmic coincidence problem. Bisabr [20] has studied the holographic DE model in a generalized scalar–tensor theory. He has shown that various types of potentials, the equation of state parameter is negative and transition from deceleration to acceleration expansion of the Universe is possible. Many researchers [21–30] have studied HDE models in various theories of gravitation. In particular, Mazumder and Chakraborty [31] have investigated the validity of the generalized second law of thermodynamics of the universe bounded by the event horizon in the holographic DE model. Setare and Jamil [32] have presented a detailed discussion on statefinder diagnostic and stability of modified gravity consistent with holographic and agegraphic DE. Sharif and Khanum [33] have investigated the Kaluza–Klein (KK) cosmology in which modified holographic DE is interacting with DM. Further, they have shown that the generalized second law of thermodynamics holds without any constraint. Mohammadi and Malekjani [34] have discussed the entropy-corrected version of interacting holographic DE, in the non-flat Universe enclosed by apparent horizon. Two corrections of entropy so-called logarithmic and power law in this model with apparent horizon as an IR-cutoff is studied. Sharif and Jawad [35] have discussed cosmological evolution of interacting NHDE in non-flat Uni-

verse. Li et al. [36] have performed a detailed investigation on the cosmological constraints on the Holographic Dark Energy (HDE) model by using the Planck data. Praseetha and Mathew [37] have studied the cosmology and thermodynamics of HDE, and also, they have analyzed the generalized second law of thermodynamics in a flat Universe consisting of interacting DE and DM. Jawad et al. [38] have discussed the modified holographic Ricci DE model in Chameleon Brans–Dicke gravity with its energy density in interaction with energy density of Cold Dark Matter (CDM) and explored its thermodynamic consequence. Aditya and Reddy [39] have investigated anisotropic new holographic dark energy model in the framework of Saez–Ballester theory of gravitation. Very recently, Prasanthi and Aditya [40] have investigated anisotropic Renyi HDE models in the framework of general relativity. In recent years, various entropy formalisms have been used to investigate the gravitational and cosmological setups. Among them Tsallis HDE (THDE) model based on the Tsallis generalized entropy, which is never stable at the classical level [41, 42]. Hence, with this motivation, in this paper, we assume the HDE with new entropy formalism i.e., Tsallis HDE.

Here, we would like to study the difference between our work and the other THDE models studied in literature [43–53]. Zadeh et al. [43] have explored the effects of various IR cutoffs on the properties of THDE model. Sharma and Pradhan [44] have investigated diagnosing THDE models with statefinder and  $\omega_r - \omega'_r$  plane analysis. Sadri [45] and Aditya et al. [46] have studied observational constraints on interacting THDE models in Brans–Dicke scalar–tensor theory. Sharif and Saba [47], Maity and Debnath [48] and Ayman [48] have investigated different THDE models in various theories of gravitation. It is observed that all these studies are in the isotropic background of the universe, i.e., with FRW space-time. But in view of the importance of anisotropic space-times, many authors have investigated THDE models in the anisotropic background. These anisotropic models will help for a better understanding of the early stages of evolution of the Universe. Korunur [50] has studied THDE model in Bianchi type-III Universe with scalar fields. Zadeh et al. [51] explained the cosmic evolution of Bianchi type-I THDE model with sign-changeable interaction between DM and DE with various IR cutoffs. Dubey et al. [52] have discussed THDE models with Hubble horizon as IR cutoff in axially symmetric Bianchi type-I space-time whereas, Dubey et al. [53] have studied THDE in Bianchi type-I Universe using hybrid expansion law with k-essence. THDE model with anisotropic background and in the framework of Saez–Ballester scalar–tensor theory of gravitation has not been, so far, studied in literature. Hence, in our work, we studied the behavior of THDE with Hubble horizon as the IR cutoff in the background of Bianchi type-III space-time within the framework of Saez–Ballester scalar–tensor theory of gravita-

tion. We obtained an exact and viable solution by solving the field equations of our proposed THDE model without considering any spacial expansion law for average scale factor of the model.

The plan of this work as follows: in Sect. 2 we have derived SB field equations with the help of Bianchi type-III metric in the presence of two minimally interacting fields: DM and THDE components. Section 3 devoted to the cosmological solution of the field equations. Also, we have constructed non-interacting and interacting THDE models along with their physical discussions. In Sect. 4, we presented a comparative analysis of our work with the recent works on THDE and with the modern observational data. In the last section, we have summarized our results.

### 2 Metric and SB field equations

We consider the spatially homogeneous and anisotropic Bianchi type-III space-time described by the following metric

$$ds^2 = dt^2 - A^2(t)dx^2 - B^2(t)e^{-2x}dy^2 - C^2(t)dz^2, \tag{4}$$

where  $A(t)$ ,  $B(t)$ , and  $C(t)$  represent the metric potentials of the Universe.

The Saez–Ballester field equations for combined matter and DE are given by

$$R_{ij} - \frac{1}{2}Rg_{ij} - w\phi^n \left( \phi_{,i}\phi_{,j} - \frac{1}{2}g_{ij}\phi_{,k}\phi^{,k} \right) = -(T_{ij} + \bar{T}_{ij}), \tag{5}$$

and the scalar fields ( $\phi$ ) satisfies the Eq. (2). We have energy conservation equation as

$$(T_{ij} + \bar{T}_{ij})_{;j} = 0. \tag{6}$$

Here the energy–momentum tensor for matter ( $T_{ij}$ ) and THDE ( $\bar{T}_{ij}$ ) are given as follows:

$$T_{ij} = \rho_m u_i u_j = \text{diag}[1, 0, 0, 0]\rho_m, \tag{7}$$

$$\bar{T}_{ij} = (p_t + \rho_t)u_i u_j - p_t g_{ij} = \text{diag}[1, -\omega_t, -\omega_t, -\omega_t]\rho_t, \tag{8}$$

it can be parameterized as

$$\bar{T}_{ij} = \text{diag}[1, -\omega_t, -\omega_t, -(\omega_t + \gamma)]\rho_t, \tag{9}$$

where  $\rho_t$ ,  $\rho_m$  are energy densities of THDE and matter, respectively and  $p_t$  is the pressure of THDE.  $\omega_t = \frac{p_t}{\rho_t}$  is

an equation of state (EoS) parameter. Here  $\gamma$  is the deviation from EoS parameter in  $z$  direction, known as skewness parameter.

The SB field equations for Bianchi type-III universe (4) with the help of Eq. (5) can be written as

$$\frac{\ddot{B}}{B} + \frac{\ddot{C}}{C} + \frac{\dot{B}\dot{C}}{BC} - \frac{w}{2}\phi^n \dot{\phi}^2 = -\omega_t \rho_t, \tag{10}$$

$$\frac{\ddot{A}}{A} + \frac{\ddot{C}}{C} + \frac{\dot{A}\dot{C}}{AC} - \frac{w}{2}\phi^n \dot{\phi}^2 = -\omega_t \rho_t, \tag{11}$$

$$\frac{\ddot{A}}{A} + \frac{\ddot{B}}{B} + \frac{\dot{A}\dot{B}}{AB} - \frac{1}{A^2} - \frac{w}{2}\phi^n \dot{\phi}^2 = -(\omega_t + \gamma) \rho_t, \tag{12}$$

$$\frac{\dot{A}\dot{B}}{AB} + \frac{\dot{B}\dot{C}}{BC} + \frac{\dot{A}\dot{C}}{AC} - \frac{1}{A^2} + \frac{w}{2}\phi^n \dot{\phi}^2 = \rho_m + \rho_t, \tag{13}$$

$$\frac{\dot{A}}{A} - \frac{\dot{B}}{B} = 0, \tag{14}$$

$$\ddot{\phi} + \left( \frac{\dot{A}}{A} + \frac{\dot{B}}{B} + \frac{\dot{C}}{C} \right) \dot{\phi} + \frac{n}{2} \frac{\phi^2}{\phi} = 0. \tag{15}$$

We can write the continuity equation (6) of the matter and THDE as

$$\dot{\rho}_m + \dot{\rho}_t + \left( \frac{\dot{A}}{A} + \frac{\dot{B}}{B} + \frac{\dot{C}}{C} \right) (\rho_m + (1 + \omega_t)\rho_t) + \gamma \frac{\dot{C}}{C} \rho_t = 0, \tag{16}$$

where overhead dot (.) denotes for ordinary differentiation with respect to  $t$ .

### 3 Solution of field equations and cosmological models

From Eq. (14), we have

$$A = B. \tag{17}$$

In view of Eq. (17), the field equations (10)–(15) constitute a system of four independent equations with six unknowns:  $A$ ,  $C$ ,  $\rho_m$ ,  $\omega_t$ ,  $\phi$  and  $\gamma$ . Hence, in order to find the determinate solution of the non-linear field equations we use the following plausible physical condition:

The shear scalar ( $\sigma^2$ ) is proportional to the scalar expansion ( $\theta$ ) which leads to a relationship between metric potentials [54]

$$A = C^k \tag{18}$$

where  $k \neq 1$  is a positive constant which preserves the non-isotropic behavior of the space-time.

Now from Eqs. (10), (11), (17) and (18), we get

$$\frac{\ddot{C}}{C} + 2k \frac{\dot{C}}{C} = \frac{1 - \gamma \rho_t C}{(k - 1) \dot{C}} \tag{19}$$

in order to solve this Eq. (19), we use the physically viable assumption as given below

$$\gamma = \frac{1 - (k - 1)\gamma_0 \dot{C}}{C\rho_t} \tag{20}$$

where  $\gamma_0$  is an arbitrary constant.

Now from Eqs. (19) and (20), we get the metric potentials

$$A = B = \left( \frac{(2k + 1)c_1 e^{\gamma_0 t}}{\gamma_0} + c_2(2k + 1) \right)^{\frac{k}{2k+1}}, \tag{21}$$

$$\&C = \left( \frac{(2k + 1)c_1 e^{\gamma_0 t}}{\gamma_0} + c_2(2k + 1) \right)^{\frac{1}{2k+1}}, \tag{22}$$

where  $c_1$  and  $c_2$  are integration constants. Using the metric potentials (21) and (22) in metric (4), we can write

$$ds^2 = dt^2 - \left[ \frac{(2k + 1)c_1 e^{\gamma_0 t}}{\gamma_0} + c_2(2k + 1) \right]^{\frac{2k}{2k+1}} \times (dx^2 + e^{-2x} dy^2) - \left[ \frac{(2k + 1)c_1 e^{\gamma_0 t}}{\gamma_0} + c_2(2k + 1) \right]^{\frac{2}{2k+1}} dz^2. \tag{23}$$

Equation (23) describes Bianchi type-III Tsallis holographic dark energy cosmological model in Saez–Ballester scalar–tensor theory of gravitation along with the following properties:

The energy density of the Tsallis holographic DE is given by the following relation [42]

$$\rho_t = \alpha L^{2\delta-4} \tag{24}$$

where  $\alpha$  is a constant,  $L$  can be considered as the size of the current Universe such as the Hubble scale and the future event horizon, and  $\delta$  is a free parameter. It can be seen that  $\rho_t$  reduces to the energy density of HDE model at  $\delta = 1$ .

We consider the Hubble horizon as the IR cutoff of the system  $L = H^{-1}$ , where  $H$  is the Hubble parameter of the model. Hence, in SB theory the energy density (24) takes the form

$$\rho_t = \alpha H^{4-2\delta}. \tag{25}$$

For our model, the Hubble parameter ( $H$ ) can be obtained as

$$H = \frac{1}{3} \left( 2 \frac{\dot{A}}{A} + \frac{\dot{C}}{C} \right) = \frac{c_1(2k + 1)e^{\gamma_0 t}}{3 \left( \frac{(2k+1)}{\gamma_0} c_1 e^{\gamma_0 t} + c_2(2k + 1) \right)}. \tag{26}$$

From Eqs. (25) and (26), we get the energy density of the THDE as

$$\rho_t = \alpha \left[ \frac{c_1(2k + 1)e^{\gamma_0 t}}{3 \left( \frac{(2k+1)}{\gamma_0} c_1 e^{\gamma_0 t} + c_2(2k + 1) \right)} \right]^{4-2\delta}. \tag{27}$$

Using Eqs. (21), (22), (26), (27) in (12), we get the energy density of the matter in terms of Hubble parameter as

$$\rho_m = \frac{9k(k + 2)}{(2k + 1)^2} H^2 - \left( \frac{c_1(2k + 1)e^{\gamma_0 t}}{3H} \right)^{\frac{-2k}{2k+1}} + \frac{w\phi_0^2}{2} \frac{9H^2 e^{-2\gamma_0 t}}{c_1^2(2k + 1)^2} - \alpha H^{4-2\delta}. \tag{28}$$

Using Eqs. (21) and (22) in (15) and (20) we get the SB scalar field  $\phi$  as

$$\phi^{\frac{n+2}{2}} = \frac{n + 2}{2} \int \phi_0 \left( \frac{(2k + 1)}{\gamma_0} c_1 e^{\gamma_0 t} + c_2(2k + 1) \right)^{-1} dt + c_4, \tag{29}$$

where  $\phi_0$  and  $c_4$  are integration constants.

$$\gamma = \frac{1 - (k - 1)c_1 \gamma_0 e^{\gamma_0 t} \left( \frac{(2k+1)}{\gamma_0} c_1 e^{\gamma_0 t} + c_2(2k + 1) \right)^{\frac{-1}{2k+1}}}{\rho_t \left( \frac{(2k+1)}{\gamma_0} c_1 e^{\gamma_0 t} + c_2(2k + 1) \right)^{\frac{2k}{2k+1}}} \tag{30}$$

In Fig. 1, we have plotted the behavior of skewness parameter ( $\gamma$ ) versus redshift ( $z$ ) for the different values of  $\gamma_0 = 2.13, 2.23, 2.33$ . We observe that skewness parameter is positive throughout evolution of the Universe. It can be seen that at initial epoch it increases, reaches a maximum value at present epoch and vanishes at late times. Also, as  $\gamma_0$  increases the skewness parameter value increases. The Figs. 2 and 3 represent the plots of energy density ( $\rho_m$ ) of matter and THDE with the Hubble horizon cutoff against redshift ( $z$ ) for the values, respectively. It is observed that both  $\rho_m$  and  $\rho_t$  are positive and decrease as universe evolves.

In the coming sections, we consider the two cases: Non-interacting model and interacting model. We determine in both the cases, energy density of THDE  $\rho_t$ , EoS parameter  $\omega_t$ , squared sound speed  $v_s^2$  and  $\omega_t - \omega'_t$  plane by solving the SB field equations. We also discussed their physical behavior.

### 3.1 Non-interacting model

Firstly, we consider that there is no energy exchange between the two components (dark sectors), and hence, the energy conservation equation (16) leads us to the following separate conservation equations:

$$\dot{\rho}_m + 3H\rho_m = 0, \tag{31}$$

$$\dot{\rho}_t + 3H(1 + \omega_t)\rho_t + \gamma \frac{\dot{C}}{C}\rho_t = 0. \tag{32}$$

**Fig. 1** Plot of skewness parameter ( $\gamma$ ) versus redshift ( $z$ ) for  $c_1 = 0.01$ ,  $c_2 = 0.115$ ,  $k = 0.325$  and  $\alpha = 0.06$

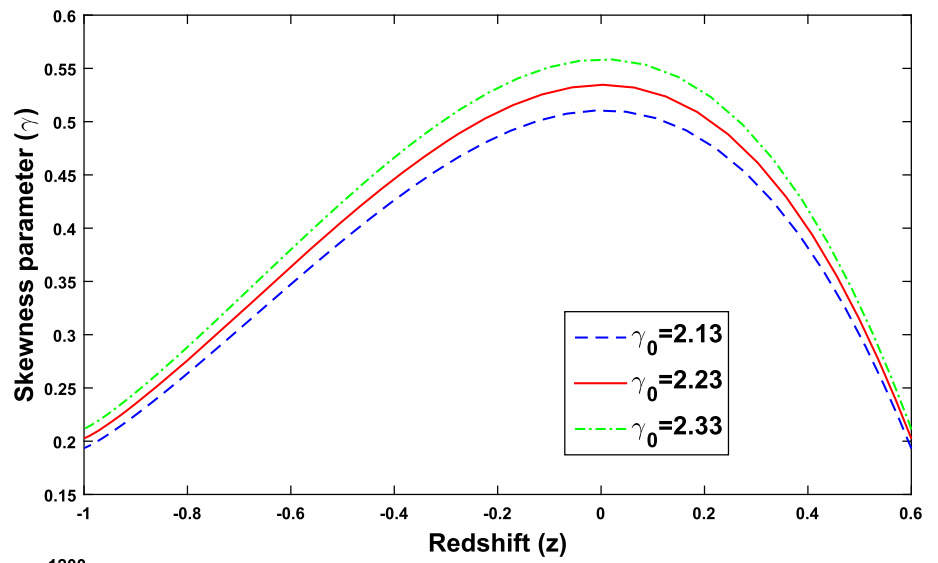


**Fig. 2** Plot of energy density ( $\rho_m$ ) of matter versus redshift ( $z$ ) for  $c_1 = 0.01$ ,  $c_2 = 0.115$ ,  $k = 0.325$ ,  $\gamma_0 = 2.13$ ,  $w = 100$ , and  $\phi_0 = 1$

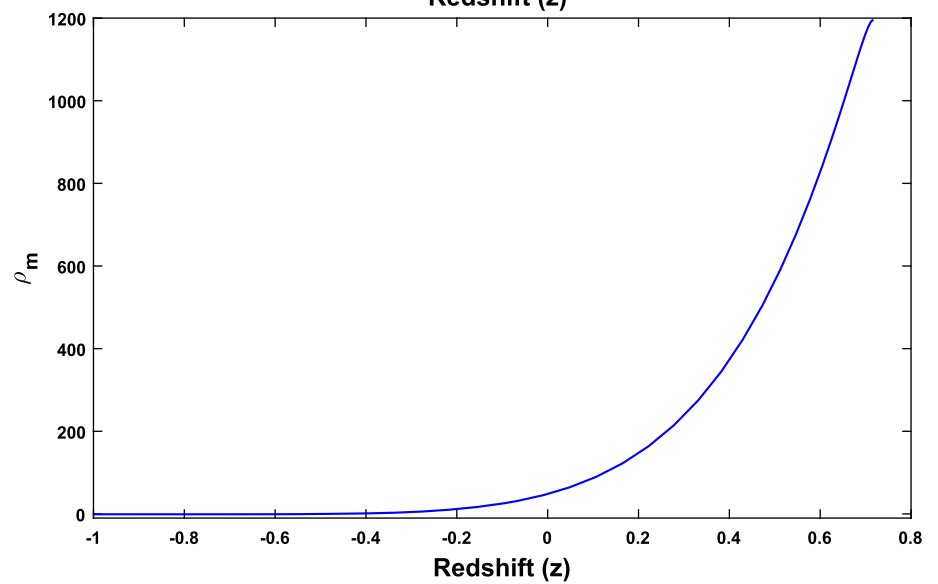
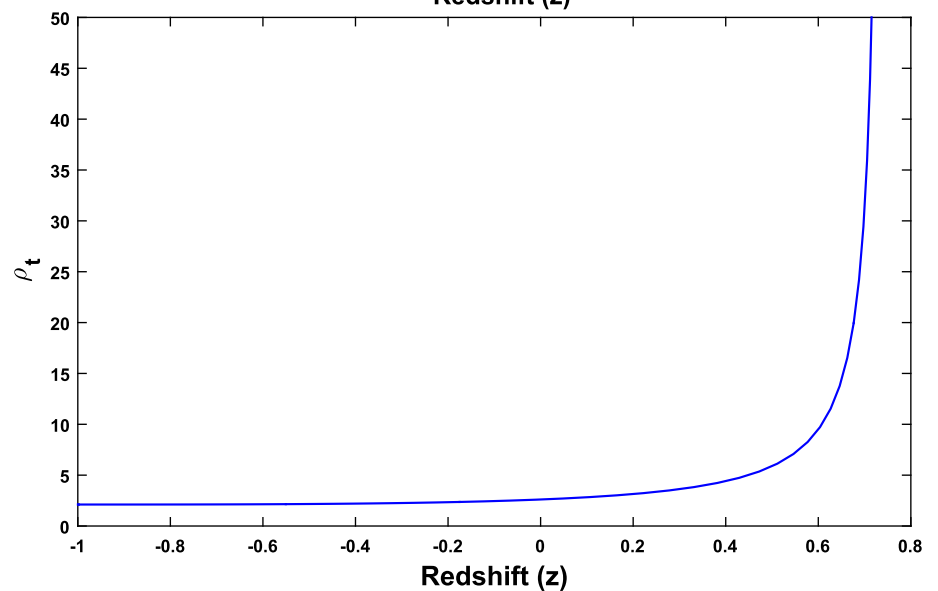


**Fig. 3** Plot of energy density ( $\rho_t$ ) of THDE versus redshift ( $z$ ) for  $c_1 = 0.01$ ,  $c_2 = 0.115$ ,  $k = 0.325$ ,  $\gamma_0 = 2.13$ ,  $\delta = 2.5$  and  $\alpha = 1.5$



Using Eqs. (26), (27) and (30) in Eq. (32), we get the EoS parameter of THDE as

$$\omega_t = -1 + \frac{3(k^2 - 1)H^{2(\delta-1)}}{(2k + 1)^2\gamma_0\alpha} - \frac{(k + 1)\left(\frac{3}{2k+1}\right)^{\frac{4k+1}{2k+1}}}{(c_1 e^{\gamma_0 t})^{\frac{2k}{2k+1}}} H^{\frac{2k\delta+2\delta-4k-3}{2k+1}} - \frac{(4 - 2\delta)\dot{H}H}{3} + \frac{(c_1(2k + 1)e^{\gamma_0 t})^{\frac{1}{2k+1}}(3H)^{\frac{2k}{2k+1}} - 3(k - 1)c_1\gamma_0 e^{\gamma_0 t} H}{c_1(2k + 1)^2 e^{\gamma_0 t}}, \tag{33}$$

where  $\dot{H} = \frac{c_1 c_2 (2k+1)^2 \gamma_0 t}{3 \left[ \left( \frac{2k+1}{\gamma_0} \right) c_1 e^{\gamma_0 t} + c_2 (2k+2) \right]^2}$ .

Caldwell and Linder [55] have pointed out that the quintessence phase of DE can be separated into two distinct regions, i.e., thawing ( $\omega_t' > 0, \omega_t < 0$ ) and freezing ( $\omega_t' < 0, \omega_t < 0$ ) regions through  $\omega_t - \omega_t'$  plane. Taking the derivative of Eq. (33) with respect to  $\ln a$ , we get

$$\omega_t' = \frac{6(k^2 - 1)}{\gamma_0\alpha(2k + 1)^2} H^{2\delta-4} \dot{H} - \left( \frac{4 - 2\delta}{3} \right) \left( \ddot{H} + \frac{\dot{H}^2}{H} \right) - \left( \left( \frac{k + 1}{c_1} \right)^{\frac{2k}{2k+1}} \left( \frac{3}{2k + 1} \right)^{\frac{4k+1}{2k+1}} \right) \times \left( \frac{2k\delta + 2\delta - 4k - 3}{2k + 1} \frac{\dot{H}}{H} - 2k\delta \right) \frac{e^{-\frac{2k\gamma_0 t}{2k+1}}}{2k + 1} H^{\frac{2k\delta+2\delta-6k-4}{2k+1}} + \frac{e^{-\gamma_0 t}}{c_1(2k + 1)^2} \left[ (c_1(2k + 1)e^{\gamma_0 t})^{\frac{1}{2k+1}} (3)^{\frac{2k}{2k+1}} ((1 - \gamma_0)H)^{\frac{2k}{2k+1}} + \frac{2k}{2k + 1} H^{\frac{-1}{2k+1}} \dot{H} \right] - 3c_1(k - 1)\gamma_0 e^{\gamma_0 t} (\gamma_0 H + \dot{H}) + 3c_1\gamma_0^2(k - 1)e^{\gamma_0 t} H, \tag{34}$$

where  $\ddot{H} = \frac{\gamma_0 c_1 c_2 (2k+1)^3 (c_2 \gamma_0 - c_1 e^{\gamma_0 t}) e^{\gamma_0 t}}{3 \left( \left( \frac{2k+1}{\gamma_0} \right) c_1 e^{\gamma_0 t} + c_2 (2k+2) \right)^3}$ .

The squared sound speed ( $v_s^2$ ) is used for studying the stability of the DE models. If  $v_s^2 < 0$ , we obtain a unstable model and if  $v_s^2 > 0$ , we obtain stable model. For our non-interacting THDE model  $v_s^2$  takes the following form

$$v_s^2 = -1 + \frac{3(k^2 - 1)H^{2(\delta-1)}}{(2k + 1)^2\gamma_0\alpha} - \frac{(k + 1)\left(\frac{3}{2k+1}\right)^{\frac{4k+1}{2k+1}}}{(c_1 e^{\gamma_0 t})^{\frac{2k}{2k+1}}} H^{\frac{2k\delta+2\delta-4k-3}{2k+1}} - \left( \frac{4 - 2\delta}{3} \right) \dot{H}H + \frac{(c_1(2k + 1)e^{\gamma_0 t})^{\frac{1}{2k+1}}(3H)^{\frac{2k}{2k+1}} - 3(k - 1)c_1\gamma_0 e^{\gamma_0 t} H}{c_1(2k + 1)^2 e^{\gamma_0 t}} + \frac{1}{4 - 2\delta} \left[ \frac{6(k^2 - 1)}{\gamma_0\alpha(2k + 1)^2} H^{2\delta-3} \dot{H} - \left( \frac{4 - 2\delta}{3} \right) (H\ddot{H} + \dot{H}^2) - \left( \left( \frac{k + 1}{c_1} \right)^{\frac{2k}{2k+1}} \left( \frac{3}{2k + 1} \right)^{\frac{4k+1}{2k+1}} \right) \times \left( \left( \frac{2k\delta + 2\delta - 4k - 3}{2k + 1} \right) \frac{\dot{H}}{H} - 2k\gamma_0 \right) \frac{e^{-\frac{2k\gamma_0 t}{2k+1}}}{2k + 1} H^{\frac{2k\delta+2\delta-6k-1}{2k+1}} + \frac{e^{-\gamma_0 t}}{c_1(2k + 1)^2} \left[ (c_1(2k + 1)e^{\gamma_0 t})^{\frac{1}{2k+1}} (3)^{\frac{2k}{2k+1}} ((1 - \gamma_0)H)^{\frac{2k}{2k+1}} + \frac{2k}{2k + 1} H^{\frac{-1}{2k+1}} \dot{H} \right] - 3c_1(k - 1)\gamma_0 e^{\gamma_0 t} (\gamma_0 H + \dot{H}) + 3c_1\gamma_0^2(k - 1)e^{\gamma_0 t} H \right] \frac{H}{\dot{H}} \tag{35}$$

The behaviour of the EoS parameter ( $\omega_t$ ) versus redshift ( $z$ ) for non-interacting THDE model is depicted in the Fig. 4 for different values of  $\gamma_0$ . It can be observed that the model starts from matter dominated era, crosses quintessence and vacuum DE (CDM) model ( $\omega_t = -1$ ) and finally approached to phantom region ( $\omega_t < -1$ ). Also, we observe that as the

**Fig. 4** Plot of EoS parameter ( $\omega_t$ ) versus redshift ( $z$ ) for  $c_1 = 0.01, c_2 = 0.115, k = 0.925, \gamma_0 = 2.13, 2.23, 2.33$

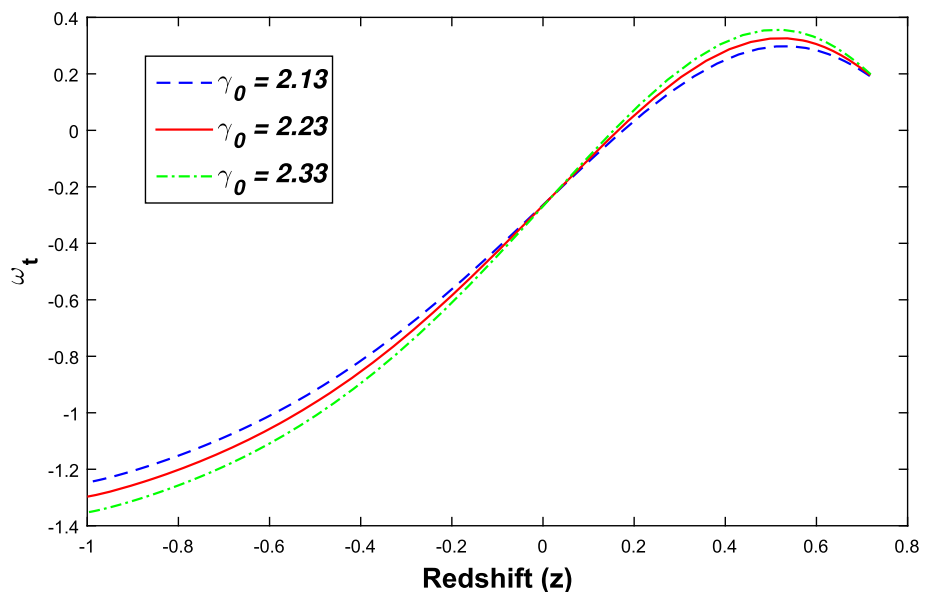


**Fig. 5** Plot of  $\omega_t$  versus  $\omega_t'$  for  $c_1 = 0.01, c_2 = 0.115, k = 0.325, \gamma_0 = 2.13,$  and  $\alpha = 1.5$

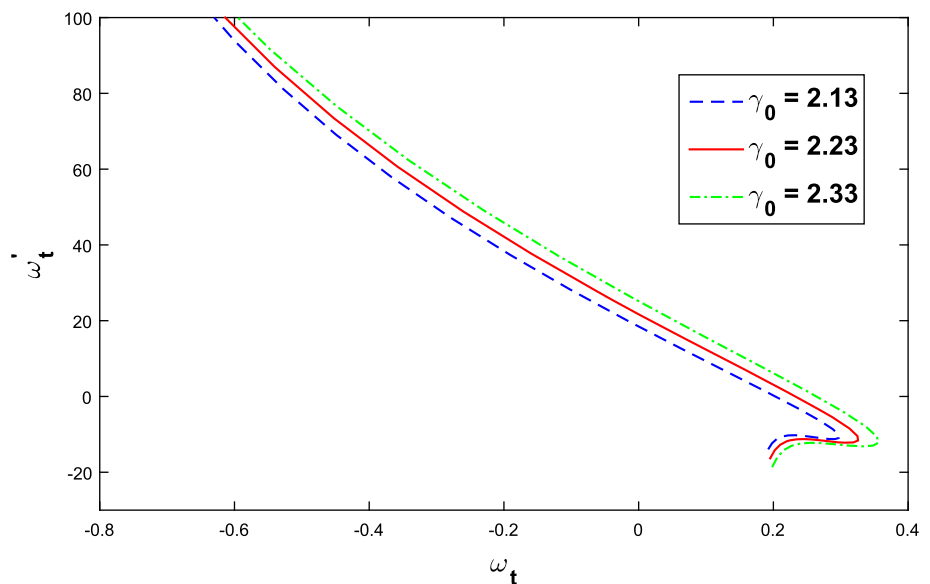
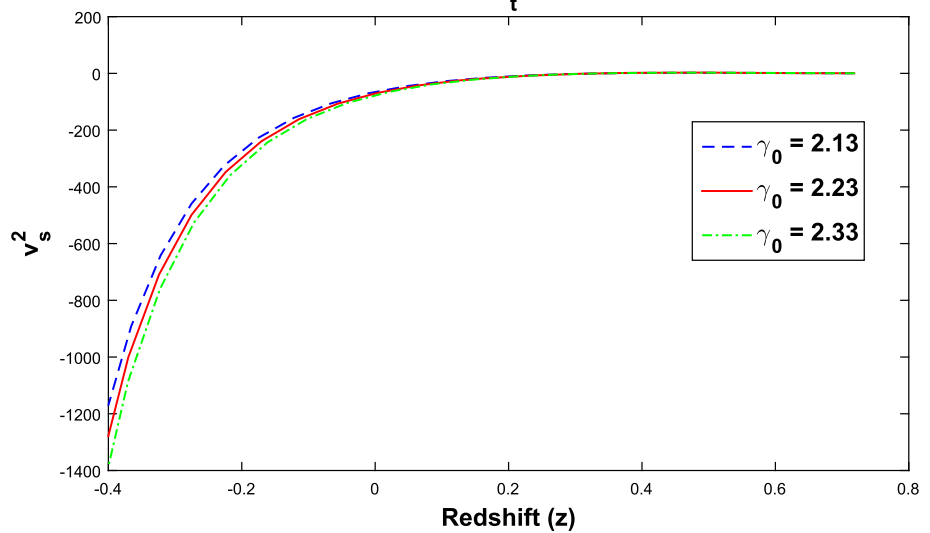


**Fig. 6** Plot of energy density of THDE versus redshift ( $z$ ) for  $c_1 = 0.01, c_2 = 0.115, k = 0.325, \gamma_0 = 2.13, 2.23, 2.33,$  and  $\alpha = 1.5$



skewness parameter increases the EoS parameter attains high phantom values.

The  $\omega_t - \omega_t'$  plane for non-interacting THDE model for different values of  $\gamma_0 = 2.13, 2.23, 2.33$  is plotted in Fig. 5. It can be observed that the  $\omega_t - \omega_t'$  plane corresponds to both thawing and freezing regions for all values of  $\gamma_0$ . This shows that the plane analysis is consistent with the accelerated expansion of the Universe.

We plot squared sound speed ( $v_s^2$ ) in terms of redshift ( $z$ ) as represented in Fig. 6. The squared speed of sound bears a decreasing behavior but with negative signature which exhibits unstable behavior of our non-interacting THDE model.

### 3.2 Interacting model

In this case, we consider the interaction between two dark components. Since the nature of both DE and DM is still unknown, there is no physical argument to exclude the pos-

sible interaction between them. Recently, some observational data shows that there is an interaction between dark sectors [56,57]. Abdalla et al. [58,59] have investigated the signature of interaction between DE and DM by using optical, X-ray and weak lensing data from the relaxed galaxy clusters. So, it is reasonable to assume the interaction between DE and DM in cosmology. For this purpose, we can write the energy conservation equations as

$$\dot{\rho}_m + 3H\rho_m = Q \tag{36}$$

$$\dot{\rho}_t + 3H(1 + \omega_t)\rho_t + \gamma \frac{\dot{C}}{C}\rho_t = -Q, \tag{37}$$

where the quantity  $Q$  denotes interaction between DE components. From the Eqs. (36) and (37), we can say that the total energy is conserved. Since there is no natural information from fundamental physics on the interaction term  $Q$ , one can only study it to a phenomenological level. Various forms of interaction term extensively considered in literature include  $Q = 3cH\rho_m, Q = 3cH\rho_{de}$  and  $Q = 3cH(\rho_m + \rho_{de})$ . Here,

**Fig. 7** Plot of EoS parameter of THDE versus redshift ( $z$ ) for  $c_1 = 0.01, c_2 = 0.115, k = 0.325, \gamma_0 = 2.13, \alpha = 1.5,$  and  $\beta = -0.10, -0.12, -0.14$

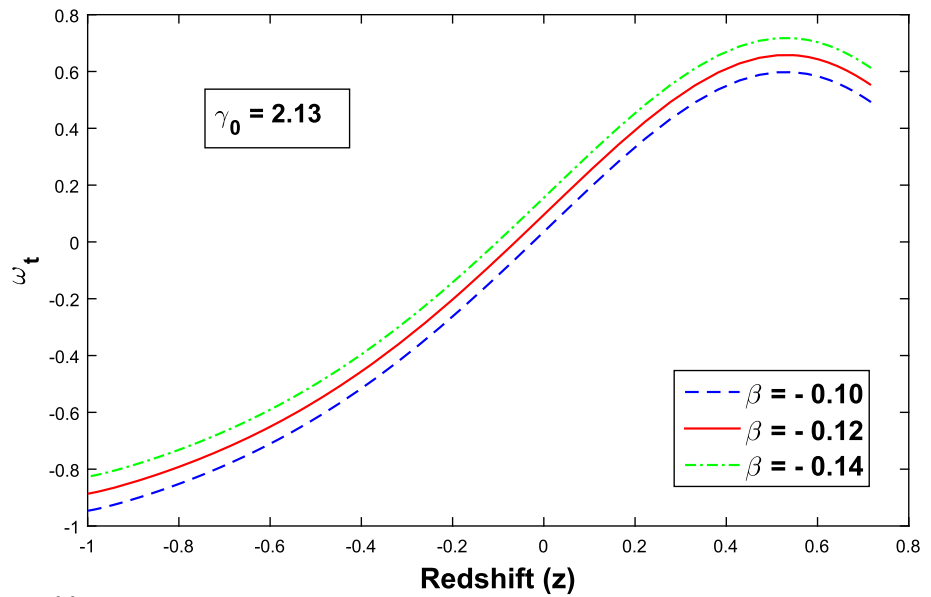
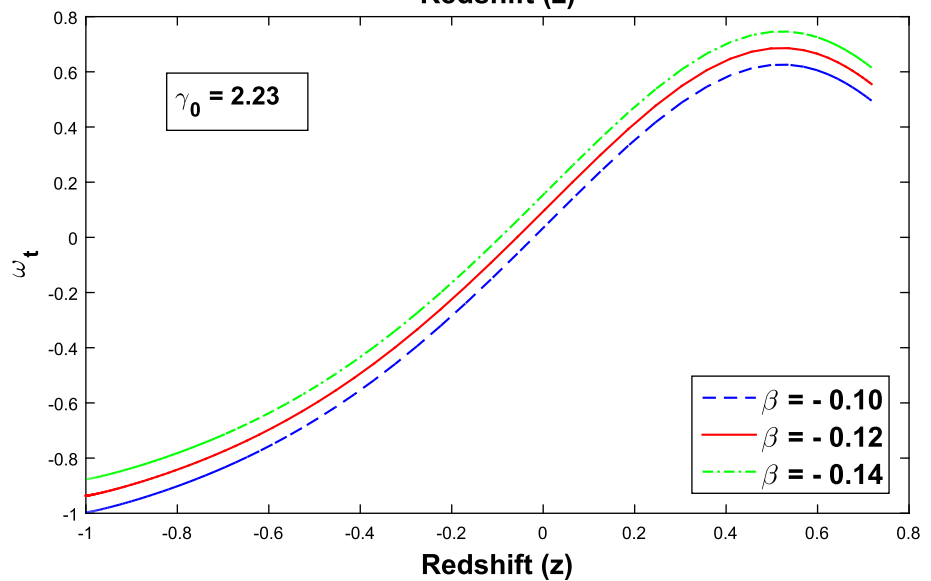


**Fig. 8** Plot of EoS parameter of THDE versus redshift ( $z$ ) for  $c_1 = 0.01, c_2 = 0.115, k = 0.325, \gamma_0 = 2.23,$  and  $\alpha = 1.5, \beta = -0.10, -0.12, -0.14$



$c$  is a coupling constant and positive  $c$  means that DE decays into DM, while negative  $c$  means DM decays into DE. Here we consider  $Q = 3\beta H\rho_t$  as the interaction term with the coupling parameter  $\beta$ .

Using Eqs. (26), (27), (30) in (36), we find that the EoS parameter

$$\begin{aligned} \omega_t = & -1 - 3\beta + \frac{3(k^2 - 1)H^{2(\delta-1)}}{(2k + 1)^2\gamma_0\alpha} \\ & - \frac{(k + 1)\left(\frac{3}{2k+1}\right)^{\frac{4k+1}{2k+1}} H^{\frac{2k\delta+2\delta-4k-3}{2k+1}}}{(c_1 e^{\gamma_0 t})^{\frac{2k}{2k+1}}} - \frac{(4 - 2\delta)}{3} \dot{H} H \\ & + \frac{(c_1(2k + 1)e^{\gamma_0 t})^{\frac{1}{2k+1}} (3H)^{\frac{2k}{2k+1}} - 3(k - 1)c_1\gamma_0 e^{\gamma_0 t} H}{c_1(2k + 1)^2 e^{\gamma_0 t}}. \end{aligned} \tag{38}$$

Three Figs. 7, 8 and 9 show that the behavior of EoS parameter for interacting THDE model versus redshift ( $z$ ) for different values of  $\gamma_0$  and  $\beta$ . It is observed that for all the considered values of  $\gamma_0$  and  $\beta$ , the model starts from matter dominated era, crosses the quintessence phase  $-1 < \omega_t < -0.33$  and finally approaches to  $\Lambda$ CDM model  $\omega_t = -1$ . Also, we observe that as  $\beta$  increases the EoS parameter of our model approaches high phantom values.

Taking the derivative of Eq. (38) with respect to  $\ln a$ , we get

**Fig. 9** Plot of EoS parameter of THDE versus redshift ( $z$ ) for  $c_1 = 0.01$ ,  $c_2 = 0.115$ ,  $k = 0.325$ ,  $\gamma_0 = 2.33$ ,  $\beta = -0.10, -0.12, -0.14$ , and  $\alpha = 1.5$

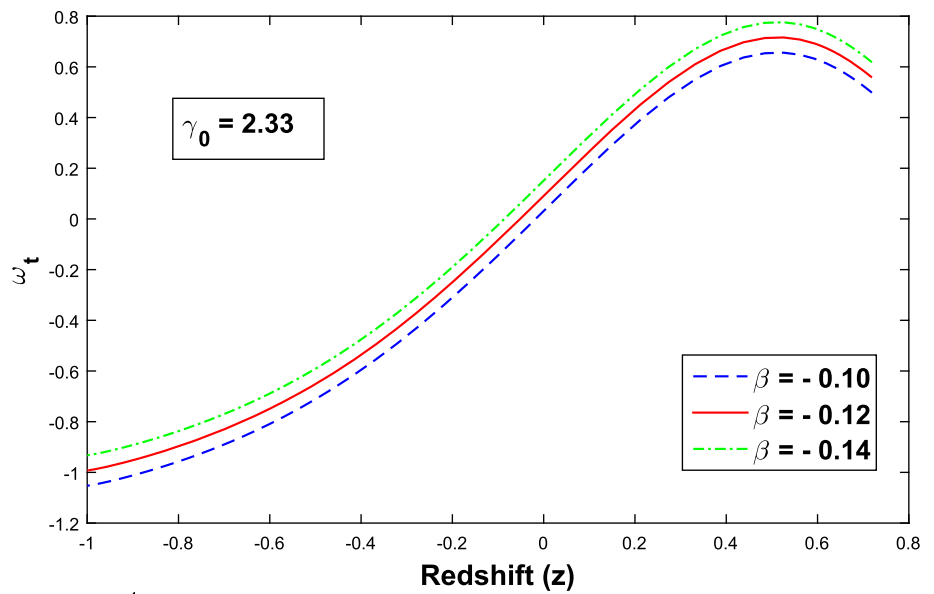


**Fig. 10** Plot of for  $c_1 = 0.01$ ,  $c_2 = 0.115$ ,  $k = 0.325$ ,  $\beta = -0.10, -0.12, -0.14$ ,  $\alpha = 1.5$ , and  $\gamma_0 = 2.13$

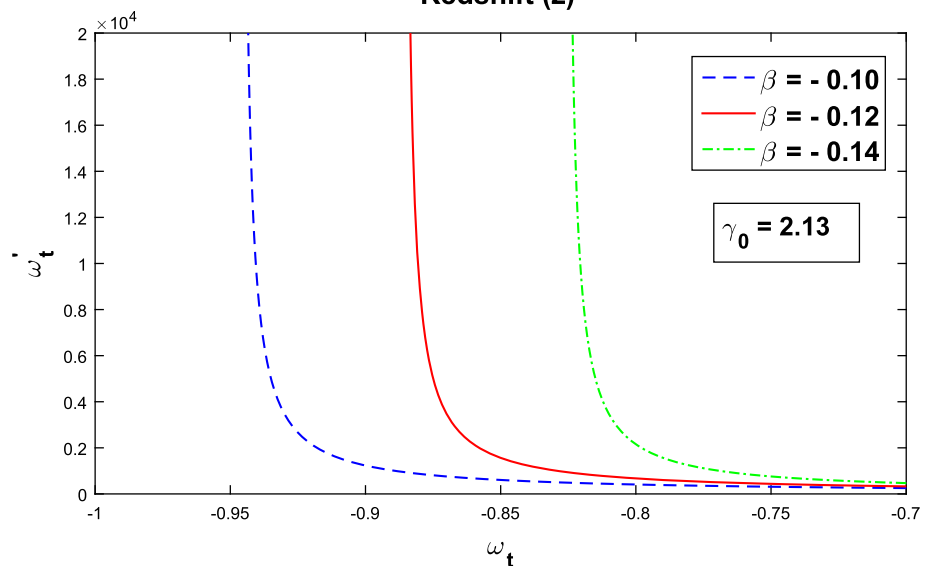
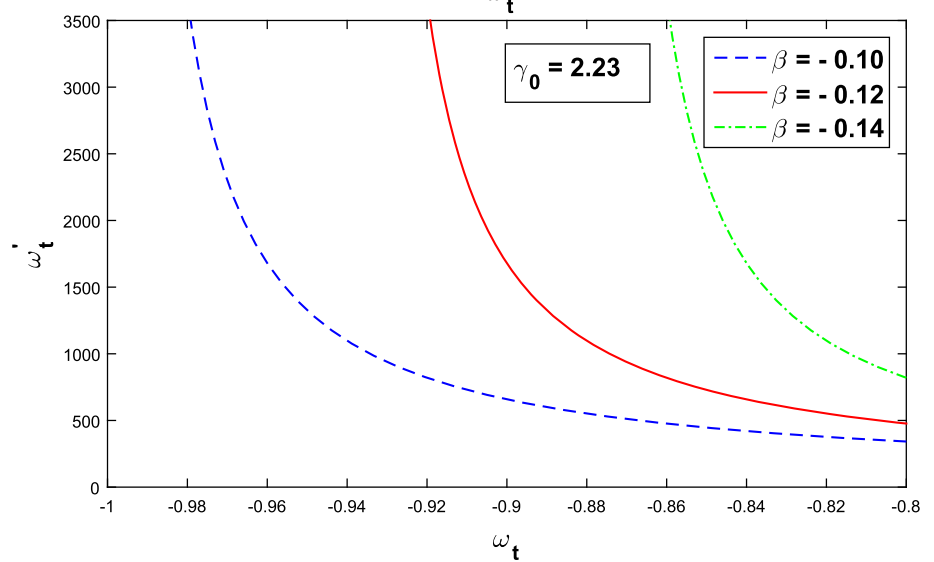


**Fig. 11** Plot of for  $c_1 = 0.01$ ,  $c_2 = 0.115$ ,  $k = 0.325$ ,  $\beta = -0.10, -0.12, -0.14$ ,  $\alpha = 1.5$ , and  $\gamma_0 = 2.23$



$$\begin{aligned} \omega'_t = & \frac{6(k^2 - 1)}{\gamma_0 \alpha (2k + 1)^2} H^{2\delta - 4} \dot{H} - \left( \frac{4 - 2\delta}{3} \right) \left( \ddot{H} + \frac{\dot{H}^2}{H} \right) \\ & - \left( \left( \frac{k + 1}{c_1} \right)^{\frac{2k}{2k+1}} \left( \frac{3}{2k + 1} \right)^{\frac{4k+1}{2k+1}} e^{-\frac{2k\gamma_0 t}{2k+1}} \right) \frac{1}{2k + 1} \\ & \times \left( \frac{(2k\delta + 2\delta - 4k - 3)}{2k + 1} \frac{\dot{H}}{H} - 2k\delta \right) H^{\frac{2k\delta + 2\delta - 6k - 4}{2k+1}} \\ & + \frac{e^{-\gamma_0 t}}{c_1 (2k + 1)^2} \left[ (c_1 (2k + 1) e^{\gamma_0 t})^{\frac{1}{2k+1}} (3)^{\frac{2k}{2k+1}} \right. \\ & \times \left. \left( (1 - \gamma_0) H^{\frac{2k}{2k+1}} + \frac{2k}{2k + 1} H^{-\frac{1}{2k+1}} \dot{H} \right) \right. \\ & \left. - 3c_1 (k - 1) \gamma_0 e^{\gamma_0 t} (\gamma_0 H + \dot{H}) + 3c_1 \gamma_0^2 (k - 1) e^{\gamma_0 t} H \right], \end{aligned} \tag{39}$$

The  $\omega_t - \omega'_t$  plane for interacting THDE model for different values of  $\gamma_0$  and  $\beta$  shown in the Figs. 10, 11 and 12. It can be observed that the plane corresponds to the thawing phase  $\omega'_t > 0$  and  $\omega_t < 0$  for all considered values of  $\gamma_0$  and  $\beta$ .

The squared sound speed  $v_s^2$  in this case is obtained as

$$\begin{aligned} v_s^2 = & -1 - 3\beta + \frac{3(k^2 - 1)H^{2(\delta-1)}}{(2k + 1)^2 \gamma_0 \alpha} \\ & - \frac{(k + 1) \left( \frac{3}{2k+1} \right)^{\frac{4k+1}{2k+1}}}{(c_1 e^{\gamma_0 t})^{\frac{2k}{2k+1}}} H^{\frac{2k\delta + 2\delta - 4k - 3}{2k+1}} - \left( \frac{4 - 2\delta}{3} \right) \dot{H} H \\ & \times \frac{(c_1 (2k + 1) e^{\gamma_0 t})^{\frac{1}{2k+1}} (3H)^{\frac{2k}{2k+1}} - 3(k - 1) c_1 \gamma_0 e^{\gamma_0 t} H}{c_1 (2k + 1)^2 e^{\gamma_0 t}} \\ & + \frac{1}{(4 - 2\delta) \ddot{H}} \left[ \frac{6(k^2 - 1)}{\gamma_0 \alpha (2k + 1)^2} H^{2\delta - 3} \dot{H} \right. \\ & - \left. \left( \frac{4 - 2\delta}{3} \right) (H \ddot{H} + \dot{H}^2) \right. \\ & - \left. \left( \left( \frac{k + 1}{c_1} \right)^{\frac{2k}{2k+1}} \left( \frac{3}{2k + 1} \right)^{\frac{4k+1}{2k+1}} e^{-\frac{2k\gamma_0 t}{2k+1}} \right) H^{\frac{2k\delta + 2\delta - 6k - 1}{2k+1}} \right. \\ & \times \left. \left( \left( \frac{2k\delta + 2\delta - 4k - 3}{2k + 1} \right) \frac{\dot{H}}{H} - 2k\gamma_0 \right) \right. \\ & + \frac{e^{-\gamma_0 t}}{c_1 (2k + 1)^2} \left[ (c_1 (2k + 1) e^{\gamma_0 t})^{\frac{1}{2k+1}} (3)^{\frac{2k}{2k+1}} \right. \\ & \times \left. \left( (1 - \gamma_0) H^{\frac{2k}{2k+1}} + \frac{2k}{2k + 1} H^{-\frac{1}{2k+1}} \dot{H} \right) \right. \\ & \left. \left. - 3c_1 (k - 1) \gamma_0 e^{\gamma_0 t} (\gamma_0 H + \dot{H}) + 3c_1 \gamma_0^2 (k - 1) e^{\gamma_0 t} H \right] \right] \end{aligned} \tag{40}$$

We plot the squared sound speed in terms of redshift ( $z$ ) as represented in Figs. 13, 14, and 15. The squared speed of sound is negative and decreasing function as Universe evolves. This shows that our model is unstable.

### Deceleration parameter (DP)

The sign of DP ( $q$ ) shows whether the model either accelerates or decelerates. If  $q > 0$ , the model exhibits decelerating expansion, if  $q = 0$  a constant rate of expansion and an accelerating expansion if  $-1 < q < 0$ . The Universe exhibits exponential expansion or de Sitter expansion for  $q = -1$  and super exponential expansion for  $q < -1$ . The DP for our model, in both (non-interacting and interacting) cases, is given by

$$q = \frac{-a\ddot{a}}{\dot{a}^2} = -1 - \frac{3c_2 \gamma_0 t}{c_1 e^{\gamma_0 t}} \tag{41}$$

The plot of deceleration parameter versus redshift ( $z$ ) is shown in the Fig. 16. It indicates that  $q$  exhibits negative behavior throughout evolution and finally approaches to  $-1$ , which shows accelerating behavior. Also, it can be observed that initially our models exhibit super exponential expansion ( $q < -1$ ) and late times it approaches to exponential expansion ( $q = -1$ ).

### Statefinder parameters ( $r, s$ )

Sahni et al. [60] and Alam et al. [61] proposed a new geometrical diagnostic pair named the statefinder pair ( $r, s$ ), where  $r$  is generated from the average scale factor ( $a$ ) and its derivatives with respect to the cosmic time  $t$  up to the third order and  $s$  is a simple combination of  $r$  and this ( $r, s$ ) is defined as follows:

$$r = \frac{\ddot{a}}{aH^3}; s = \frac{r - 1}{3(q - \frac{1}{2})} \tag{42}$$

$$\begin{aligned} r = & \frac{9}{c_1^2 (2k + 1)^2} \left[ \gamma_0^2 e^{-2\gamma_0 t} \left( \left( \frac{2k + 1}{\gamma_0} \right) c_1 e^{\gamma_0 t} + c_2 (2k + 1) \right)^2 \right. \\ & - \frac{2(2k + 3)\gamma_0}{3} \\ & \left. e^{\gamma_0 t} \left( \left( \frac{2k + 1}{\gamma_0} \right) c_1 e^{\gamma_0 t} + c_2 (2k + 1) \right) - \frac{2c_1^2 (2k + 1)}{3} \right] \end{aligned} \tag{43}$$

**Fig. 12** Plot of energy density of THDE versus redshift ( $z$ ) for  $c_1 = 0.01$ ,  $c_2 = 0.115$ ,  $k = 0.325$ ,  $\beta = -0.10, -0.12, -0.14$ ,  $\alpha = 1.5$ , and  $\gamma_0 = 2.33$

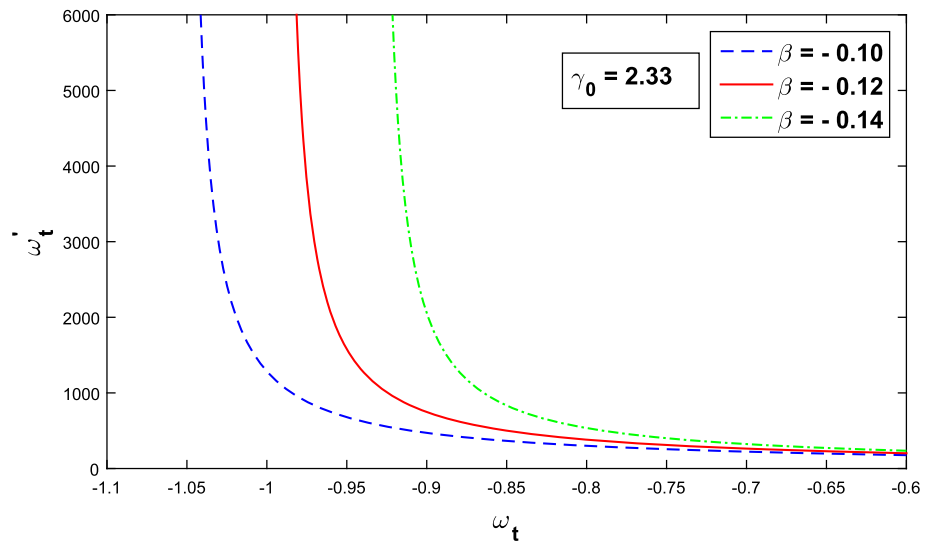


**Fig. 13** Plot of squared sound speed ( $v_s^2$ ) versus redshift ( $z$ ) for  $c_1 = 0.01$ ,  $c_2 = 0.115$ ,  $k = 0.325$ ,  $\gamma_0 = 2.13, 2.23, 2.33$ ,  $\alpha = 1.5$ , and  $\beta = -0.10$

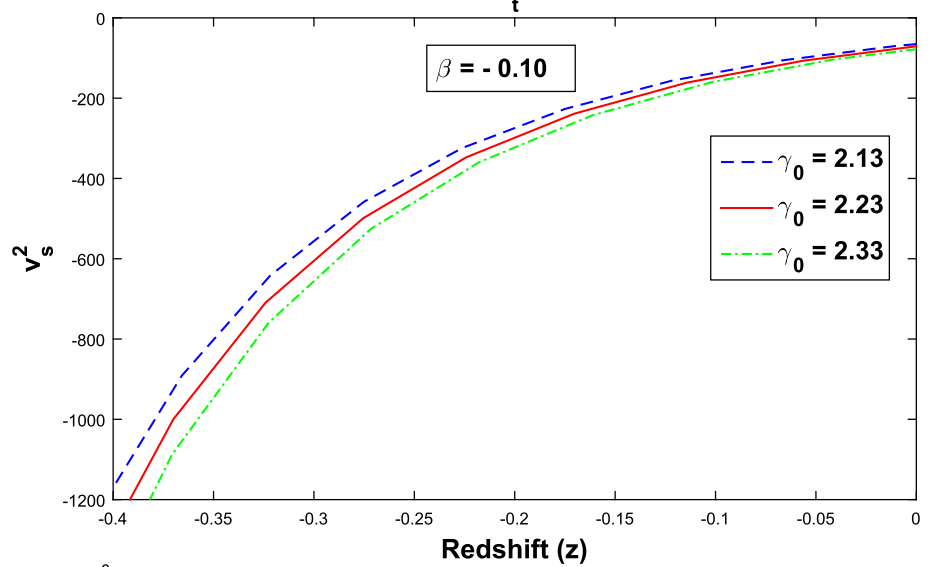


**Fig. 14** Plot of squared sound speed ( $v_s^2$ ) versus redshift ( $z$ ) for  $c_1 = 0.01$ ,  $c_2 = 0.115$ ,  $k = 0.325$ ,  $\gamma_0 = 2.13, 2.23, 2.33$ ,  $\alpha = 1.5$ , and  $\beta = -0.12$

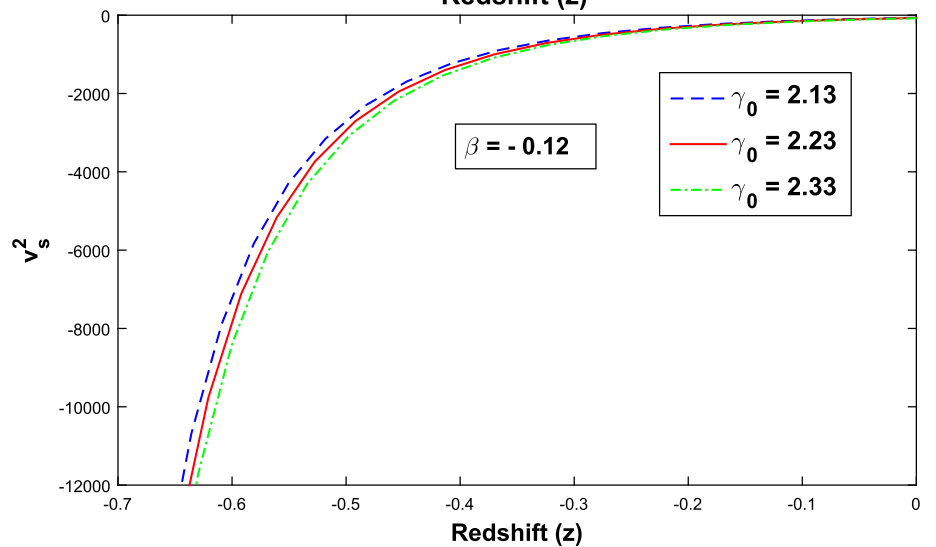


**Fig. 15** Plot of squared sound speed ( $v_s^2$ ) versus redshift ( $z$ ) for  $c_1 = 0.01$ ,  $c_2 = 0.115$ ,  $k = 0.325$ ,  $\gamma_0 = 2.13, 2.23, 2.33$ ,  $\alpha = 1.5$ , and  $\beta = -0.14$

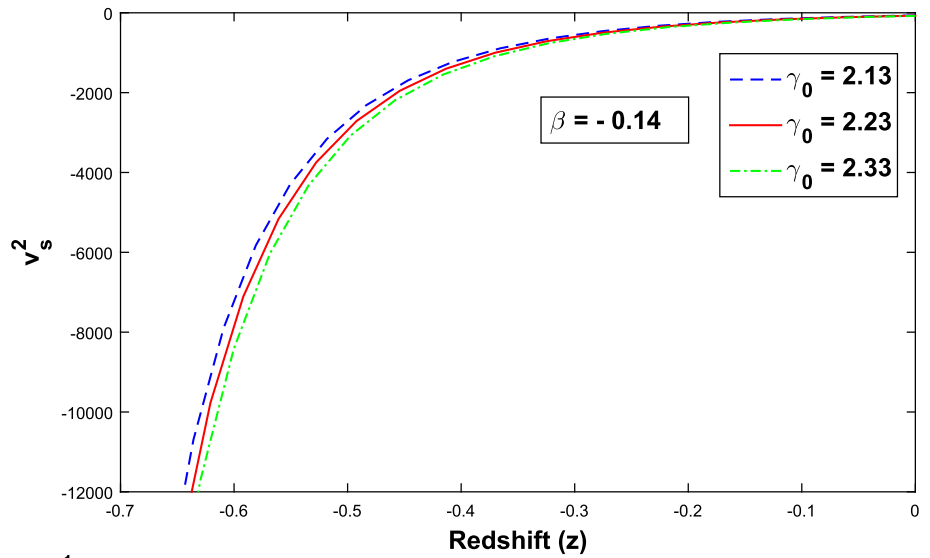


**Fig. 16** Plot of Deceleration parameter ( $q$ ) versus redshift ( $z$ ) for  $c_1 = 0.01$ ,  $c_2 = 0.115$ ,  $k = 0.325$ ,  $\gamma_0 = 2.13$

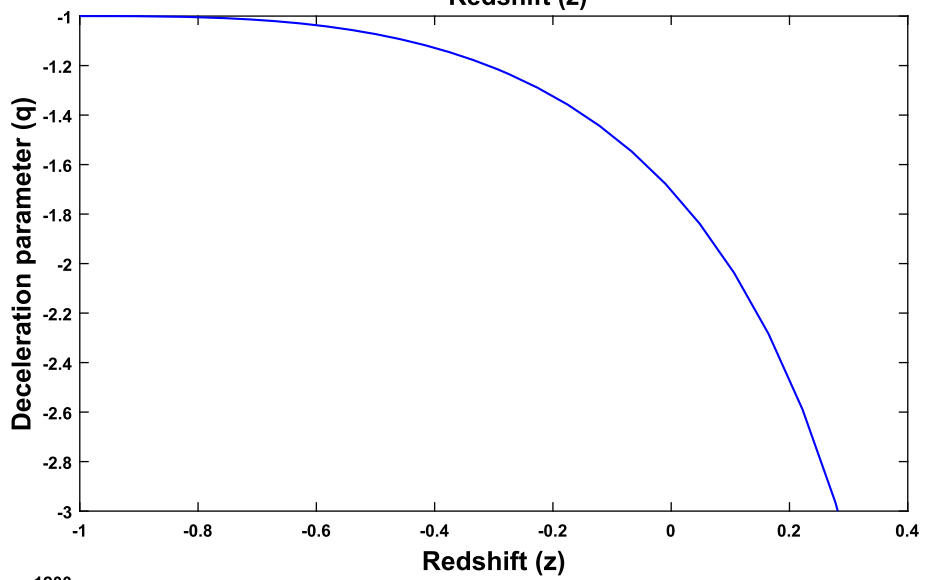
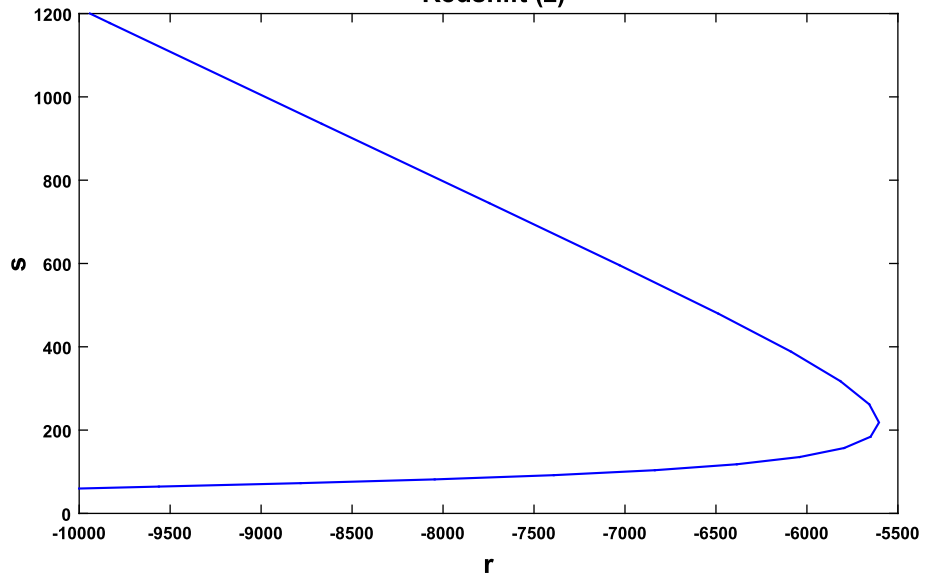


**Fig. 17** Plot of statefinder parameter ( $r, s$ ) for  $c_1 = 0.01$ ,  $c_2 = 0.115$ ,  $k = 0.325$ ,  $\gamma_0 = 2.13$



and

$$s = \left\{ \gamma_0^2 e^{-2\gamma_0 t} \left( \left( \frac{2k+1}{\gamma_0} \right) c_1 e^{\gamma_0 t} + c_2(2k+1) \right)^2 - \frac{2(2k+3)\gamma_0}{3} e^{\gamma_0 t} \left( \left( \frac{2k+1}{\gamma_0} \right) c_1 e^{\gamma_0 t} + c_2(2k+1) \right) - \frac{2c_1^2(2k+1)}{3} - \frac{c_1^2(2k+1)}{9} \right\} \left\{ \left[ \frac{1}{2} - \frac{\gamma_0}{c_1(2k+1)} e^{-\gamma_0 t} \left( \left( \frac{2k+1}{\gamma_0} \right) c_1 e^{\gamma_0 t} + c_2(2k+1) \right) - c_2(2k+1)e^{\gamma_0 t} \right] c_1^2(2k+1)^2 \right\}^{-1} \quad (44)$$

In Fig. 17, we have plotted the trajectories of the  $r - s$  plane. It can be observed that the region belongs to  $s > 0$  and  $r < 1$ . Hence our model corresponds to the DE regions such as quintessence and phantom.

*Om* diagnostic:

Sahni et al. [62] has been proposed *Om*-diagnostic parameter as a complementary to the statefinder parameter, which helps to distinguish the present matter density contrast *Om* in different models more effectively. This is also a geometrical diagnostic that explicitly depends on redshift ( $z$ ) and the Hubble parameter ( $H$ ). It is defined as follows:

$$Om(z) = \frac{\frac{H^2(z)}{H_0^2} - 1}{(1+z)^3 - 1}, \quad (45)$$

here  $H_0$  is the present value of the Hubble parameter.

We have plotted the evolution of  $Om(z)$  in the Fig. 18. It can be observed that initially the slope of  $Om(z)$  is negative and finally it approaches to positive value. Hence, our models initially behave like quintessence model and finally approaches to phantom region. We can conclude that the behavior of *Om*-diagnostic parameter coincides with the behavior of EoS parameter.

#### 4 Discussion and comparison

In this section, we present a comparative analysis of our work with the recent works on THDE and with the modern observational data.

Ghaffari et al. [63] have studied FRW THDE model in Brans–Dicke cosmology. They found that in both interacting and non-interacting THDE models, the EoS parameter approaches to the cosmological constant in future. The models are not stable. Zadeh et al. [43] have studied FRW THDE by assuming various infrared cutoffs. It is observed that the EoS parameter of interacting and non-interacting

THDE models exhibit phantom DE behavior for all the IR cutoffs. Also, they are unstable. Aditya et al. [46] have discussed observational constraints on THDE in Brans–Dicke scalar–tensor theory with logarithmic scalar field. They have investigated an EoS parameter starts from matter dominated era, then goes towards quintessence region, and finally, approaches to vacuum DE era in non-interacting case, while in interacting case, the EoS parameter starts from quintessence region and turns towards phantom region by crossing phantom divide line. Ghaffari et al. [64] have investigated THDE in fractal Universe. They have discussed an EoS parameter in non-interacting case, THDE model in the fractal universe emulates the cosmological constant while in interacting case, THDE model can cross the phantom divide line at the late time. Sharif and Saba [47] have discussed THDE models in  $f(G, T)$  gravity. They have concluded that the EoS parameter indicates phantom phase while the deceleration parameter demonstrates accelerated cosmic epoch for both conserved as well as non-conserved energy–momentum tensor. Dubey et al. [53,65] have studied Bianchi type-*I* and *III* THDE models. In both the models, the EoS parameter approaches to  $\Lambda$ CDM model in future. Dubey et al. [52] have discussed THDE models with Hubble horizon as IR cutoff in axially symmetric space-time. They have obtained an EoS parameter which varies quintessence region, crosses the phantom divide line.

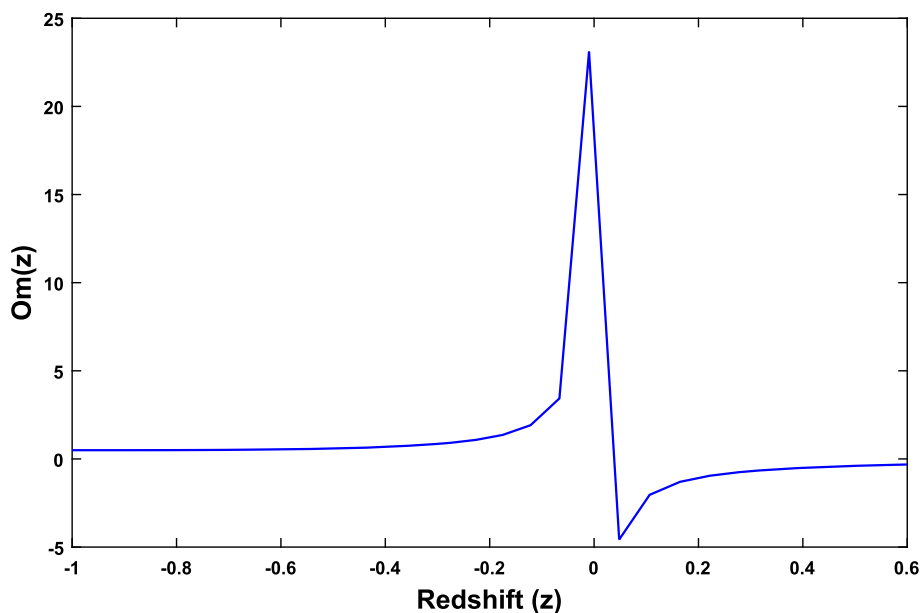
In our Bianchi type-*III* THDE models, the study of EoS parameter reveals that the model starts from matter dominated era, varies in quintessence phase and finally approaches phantom region in non-interacting case. In interacting case, the model starts from matter dominated era and finally approaches to  $\Lambda$ CDM model at late times. It can be observed that the behavior of EoS parameter in our models is coincide with the models given in the literature mentioned above. The stability analysis also coincides with the existing THDE models. The behavior of deceleration parameter coincides with the THDE model obtained by Sharif and Saba [47].

Also, it is worthwhile to mention here that the present values of EoS parameter of our DE models are in agreement with the modern Planck observational data given by Aghanim et al. [66]. It gives the constraints on EoS parameter of dark energy as follows:

$$\begin{aligned} \omega_t &= -1.56_{-0.48}^{+0.60} (Planck + TT + lowE) \\ \omega_t &= -1.58_{-0.41}^{+0.52} (Planck + TT, EE + lowE) \\ \omega_t &= -1.57_{-0.40}^{+0.50} \\ &\quad (Planck + TT, TE, EE + lowE + lensing) \\ \omega_t &= -1.04_{-0.10}^{+0.10} \\ &\quad (Planck + TT, TE, EE + lowE + lensing + BAO) \end{aligned}$$

It can be observed from the Figs. 4, and (7, 8, 9) that the EoS parameter of our models in both non-interacting and interacting cases lie within the above observational limits

**Fig. 18** Plot of  $Om$  versus redshift ( $z$ ) for  $c_1 = 0.01$ ,  $c_2 = 0.115$ ,  $k = 0.325$ ,  $\gamma_0 = 2.13$ , and  $H_0 = 1$



which shows the consistency of our results with the above cosmological data.

## 5 Conclusions

The current scenario of accelerated expansion of the universe has become an important subject of investigation. In order to explain this cosmic acceleration, two approaches have been suggested. One way is to study various dynamical DE models and the other is to consider alternative theories of gravity. Here, we have studied the accelerated expansion by assuming the THDE in Bianchi type-III universe within the framework of SB scalar-tensor theory of gravity. Using the relation between the metric potentials, we have obtained the solution of SB field equations which leads to a varying DP. We have considered interacting and non-interacting models of matter and THDE. We have also constructed different cosmological parameters to analyze the viability of these models and our conclusions are the following:

- For models, we observe that skewness parameter is positive throughout evolution of the Universe. It can be seen (Fig. 1) that at initial epoch it increases, reaches a maximum value at present epoch and vanishes at late times. Also, as  $\gamma_0$  increases the skewness parameter value increases. Skewness parameter increases with increase in the parameter  $\phi$ . It is observed from Figs. 2 and 3 both  $\rho_m$  and  $\rho_t$  are positive and decrease as universe evolves.
- It can be observed that the EoS parameter of non-interacting THDE model starts from matter dominated era, varies in quintessence era and finally approaches to phantom region ( $\omega_t < -1$ ) by crossing vacuum DE ( $\omega_t = -1$ ) for  $\gamma_0 = 2.13$ ,  $\gamma_0 = 2.23$ ,  $\gamma_0 = 2.33$ . Also,

we observe that as the skewness parameter increases the EoS parameter of our model attains maximum phantom value. The EoS parameter of interacting THDE model starts from matter dominated era, varies in quintessence phase and finally approaches to  $\Lambda$ CDM model (ref. Figs. 7, 8, 9) for all the the values of  $\gamma_0 = 2.13, 2.23, 2.33$  and  $\beta = -0.10, -0.12, -0.14$ . Finally, we observed that the EoS parameter of our models coincide with the existing THDE literature and the present values of EoS parameter lie within the modern Planck observational data.

- It can be observed that the  $\omega_t - \omega_t'$  plane corresponds to both thawing and freezing regions for all values of  $\gamma_0$  in non-interacting case, whereas in interacting case the model varies in thawing region only. However, the trajectories of  $\omega_t - \omega_t'$  plane shows consistent results with the observational data and can be considered as viable THDE models. It is observed that our both non-interacting and interacting THDE models are unstable (ref. Figs. 6, 13, 14, 15).
- The deceleration parameter, statefinder and  $Om$ -diagnostic parameters are same for both non-interacting and interacting models. It can be observed that deceleration parameter exhibits negative behavior throughout evolution and finally approaches to  $-1$ , which shows accelerating behavior (ref. Fig. 16). Also, we observed that initially our models exhibit super exponential expansion ( $q < -1$ ) and at late times it approaches to exponential expansion. This behavior coincides with the THDE model obtained by Sharif and Saba [47]. Statefinder analysis gives that our THDE model corresponds to the DE regions such as quintessence and phantom (ref. Fig. 17). We observe that the slope of  $Om(z)$  is negative, hence our models behave like quintessence model (ref. Fig. 18).

**Acknowledgements** The authors express their sincere thanks to the anonymous reviewers for their constructive comments and suggestions which have improved the presentation and quality of the manuscript.

**Data Availability Statement** This manuscript has no associated data or the data will not be deposited. [Authors' comment: All data analysed during this study are presented in this published article.]

**Open Access** This article is licensed under a Creative Commons Attribution 4.0 International License, which permits use, sharing, adaptation, distribution and reproduction in any medium or format, as long as you give appropriate credit to the original author(s) and the source, provide a link to the Creative Commons licence, and indicate if changes were made. The images or other third party material in this article are included in the article's Creative Commons licence, unless indicated otherwise in a credit line to the material. If material is not included in the article's Creative Commons licence and your intended use is not permitted by statutory regulation or exceeds the permitted use, you will need to obtain permission directly from the copyright holder. To view a copy of this licence, visit <http://creativecommons.org/licenses/by/4.0/>. Funded by SCOAP<sup>3</sup>.

## References

1. A.G. Riess et al., *Astron J.* **116**, 1009 (1998)
2. S. Perlmutter et al., *Nature* **391**, 51 (1998)
3. C.L. Bennett et al., *Astrophys. J. Suppl.* **148**, 1 (2003)
4. D.N. Spergel et al., *Astrophys. J. Suppl.* **148**, 175 (2003)
5. S.M. Carroll et al., *Living Rev. Relativ.* **4**, 1 (2001)
6. T. Padmanabhan, *Phys. Rep.* **380**, 235 (2003)
7. C. Brans, R.H. Dicke, *Phys. Rev.* **124**, 925 (1961)
8. D. Saez, V.J. Ballester, *Phys. Lett. A* **113**, 467 (1986)
9. G. 't Hooft, [arXiv:gr-qc/9310026](https://arxiv.org/abs/gr-qc/9310026) (1993)
10. L. Susskind, *J. Math. Phys.* **36**, 6377 (1995)
11. A.G. Cohen et al., *Phys. Rev. Lett.* **82**, 4971 (1999)
12. S.D.H. Hsu, *Phys. Lett. B* **594**, 13 (2004)
13. M. Li, *Phys. Lett. B* **603**, 1 (2004)
14. C. Gao et al., *Phys. Rev. D* **79**, 043511 (2009)
15. L. Granda, A. Oliveros, *Phys. Lett. B* **669**, 275 (2008)
16. S. Chen, J. Jing, *Phys. Lett. B* **679**, 144 (2009)
17. A. Sheykhi et al., *Int. J. Mod. Phys. D* **25**, 1650018 (2016)
18. S. Nojiri, S.D. Odintsov, *Gen. Relativ. Gravit.* **38**, 1285 (2006)
19. A.J.M. Medved, *Gen. Relativ. Gravit.* **41**, 287 (2009)
20. Y. Bisabr, *Gen. Relativ. Gravit.* **41**, 305 (2009)
21. D.R.K. Reddy et al., *Astrophys. Space Sci.* **361**, 349 (2016)
22. M.V. Santhi et al., *Astrophys. Space Sci.* **361**, 142 (2016)
23. M.V. Santhi et al., *Can. J. Phys.* **95**, 381 (2017a)
24. M.V. Santhi et al., *Int. J. Theor. Phys.* **56**, 362 (2017b)
25. M.V. Santhi et al., *Can. J. Phys.* **95**, 179 (2017c)
26. S.K. Tripathy, B. Mishra, P.K. Sahoo, *Eur. Phys. J. Plus* **132**, 388 (2017)
27. V.U.M. Rao et al., *Int. J. Pure Appl. Math.* **117**, 383 (2017)
28. V.U.M. Rao et al., *Results Phys.* **10**, 469 (2018)
29. Y. Aditya, D.R.K. Reddy, *Eur. Phys. J. C* **78**, 619 (2018a)
30. Y. Aditya, D.R.K. Reddy, *Astrophys. Space Sci.* **363**, 207 (2018b)
31. N. Mazumder, S. Chakraborty, *Gen. Relativ. Gravit.* **42**, 813 (2010)
32. M.R. Setare, M. Jamil, *Gen. Relativ. Gravit.* **43**, 293 (2011)
33. M. Sharif, F. Khanum, *Gen. Relativ. Gravit.* **43**, 2885 (2011)
34. A.K. Mohammadi, M. Malekjani, *Gen. Relativ. Gravit.* **44**, 1163 (2012)
35. M. Sharif, A. Jawad, [arXiv:1212.0129v1](https://arxiv.org/abs/1212.0129v1) (2012)
36. M. Li et al., *J. Cosmol. Astropart. Phys.* **9**, 021 (2013)
37. P. Praseetha, T.K. Mathew, *Class. Quantum Gravity* **31**, 185012 (2014)
38. A. Jawad et al., *Commun. Theor. Phys.* **63**, 453 (2015)
39. Y. Aditya, D.R.K. Reddy, *Astrophys Space Sci* **363**, 207 (2018)
40. U.Y. Divya Prasanthi, Y. Aditya, *Results Phys.* **17**, 103101 (2020)
41. M. Tavayef et al., *Phys. Lett. B* **781**, 195 (2018)
42. C. Tsallis, L.J.L. Cirto, *Eur. Phys. J. C* **73**, 2487 (2013)
43. M.A. Zadeh et al., *Eur. Phys. J. C* **78**, 940 (2018)
44. U.K. Sharma, A. Pradhan, *Mod. Phys. Lett. A* **34**, 1950101 (2019)
45. E. Sadri, *Eur. Phys. J. C* **79**, 762 (2019)
46. Y. Aditya et al., *Eur. Phys. J. C* **79**, 1020 (2019)
47. M. Sharif, S. Saba, *Symmetry* **11**, 92 (2019)
48. S. Maity, U. Debnath, *Eur. Phys. J. Plus* **134**, 514 (2019)
49. A.A. Aly, *Eur. Phys. J. Plus* **134**, 335 (2019)
50. M. Korunur, *Mod. Phys. Lett. A* **34**, 1950310 (2019)
51. M. A. Zadeh, et al., preprint, [arXiv:1901.05298](https://arxiv.org/abs/1901.05298) (2019)
52. V.C. Dubey et al., *Int. J. Geom. Methods Mod. Phys.* **17**, 2050011 (2020)
53. V.P. Dubey et al., *Pramana J. Phys.* **93**, 78 (2019)
54. C.B. Collins et al., *Gen. Relativ. Gravit.* **12**, 805 (1980)
55. R.R. Caldwell, E.V. Linder, *Phys. Rev. Lett.* **95**, 141301 (2005)
56. O. Bertolami et al., *Phys. Lett. B* **654**, 165 (2007)
57. O. Bertolami et al., *Gen. Relativ. Gravit.* **41**, 2839 (2009)
58. E. Abdalla et al., *Phys. Lett. B* **673**, 107 (2009)
59. E. Abdalla et al., *Phys. Rev. D* **82**, 023508 (2010)
60. V. Sahni et al., *JETP Lett.* **77**, 201 (2003)
61. U. Alam et al., *Mon. Not. R. Astron. Soc.* **344**, 1057 (2003)
62. V. Sahni, A. Shaleloo, A.A. Starobinsky, *Phys. Rev. D* **78**, 103502 (2008)
63. S. Ghaffari et al., *Eur. Phys. J. C* **78**, 706 (2018)
64. S. Ghaffari et al., *Mod. Phys. Lett. A* **20150107** (2020)
65. U.K. Sharma et al., *Int. J. Geom. Methods Mod. Phys.* **17**, 2050098 (2020)
66. N. Aghanim, et al., [Plancks Collaboration] [arXiv:1807.06209v2](https://arxiv.org/abs/1807.06209v2) (2018)